Proceedings of the ASME 2010 3rd Joint US-European Fluids Engineering Summer Meeting and 8th International Conference on Nanochannels, Microchannels, and Minichannels
FEDSM-ICNMM2010
August 1-5, 2010, Montreal, Canada

FEDSM-ICNMM2010-30845

THE MICROFLUIDIC TRAPPING OF ANTIBODY-SECRETING CELLS

Sean F. Romanuik
Simon Fraser University
School of Engineering Science
Microinstrumentation Laboratory
Burnaby, British Columbia,
V5A 1S6, Canada
sromanui@sfu.ca

Samantha M. Grist
Simon Fraser University
School of Engineering Science
Microinstrumentation Laboratory
Burnaby, British Columbia,
V5A 1S6, Canada
smg2@sfu.ca

Moeed Haq
Simon Fraser University
School of Engineering Science
Microinstrumentation Laboratory
Burnaby, British Columbia,
V5A 1S6, Canada
moeed.haq@mail.mcgill.ca

Bonnie L. Gray
Simon Fraser University
School of Engineering Science
Microinstrumentation Laboratory
Burnaby, British Columbia,
V5A 1S6, Canada
bgray@sfu.ca

Naveed Gulzar
Simon Fraser University
Department of Molecular
Biology and Biochemistry
Burnaby, British Columbia,
V5A 1S6, Canada
ngulzar@sfu.ca

Jamie K. Scott
Simon Fraser University
Department of Molecular
Biology and Biochemistry
Faculty of Health Sciences
Burnaby, British Columbia,
V5A 1S6, Canada
jkscott@sfu.ca

ABSTRACT

Therapeutic antibodies (Abs) are a rapidly growing and economically promising biotechnological research area. Therapeutic Ab production typically involves screening large numbers of Ab-secreting cells (ASCs) in order to identify those producing Abs targeting a specific antigen (Ag) with the highest affinity; a process often requiring weeks to complete. We are contributing to a multidisciplinary project focused upon the development of an immunobiosensing array ultimately intended to directly monitor the Ag-specific Ab production by thousands of ASCs on a single slide in real-time. Each ASC shall be microfluidically guided and trapped near a surface plasmon (SP) resonant nanohole array sensor so as to detect the binding of secreted Abs to Ag immobilized onto the sensor's surface. This paper presents the initial progress of our contribution to this project: the development of polymeric microfluidic devices to guide and trap large ASC populations within arrays of single-cell traps. More specifically, this paper presents several different polymer-based microfluidic trapping devices, based upon perfusive flow-through cell traps and microwells which trap settling cells, which have been evaluated using COMSOL® simulations and tested using microsphere- and cell-based flow experiments. Our initial results are promising, and verify the functionality of our microfluidic cell trap designs.

INTRODUCTION

In response to pathogenic infection or immunization, B cells (a subset of lymphocytes of the immune system) differentiate into antibody-secreting cells (ASCs) that produce proteins known as antibodies (Abs). Abs bind to molecules known as antigens (Ags). Abs that bind to specific Ags on pathogens can block their functionality and/or flag the said Ag, and thus its associated pathogen, for clearance by the immune system. As such, the secretion of Ag-specific Abs *in vivo* is a key component of an individual's humoral response and protective immunity. The development of humoral memory, *i.e.* the secretion of Ag-specific Abs in the absence of persistent Ag over long periods of time, provides an individual with protective immunity against invading pathogens and is a biological indicator of an individual's past pathogenic exposure [1,2].

There is a growing interest in the therapeutic use of human or humanized monoclonal Abs that specifically bind to Ags related to human diseases. For over twenty-five years, biotechnologists have investigated therapeutic Abs that can, with impressive selectivity: block molecules from binding to cellular receptors, initiate the complement-mediated removal of flagged Ags, recruit immune cells to destroy bound pathogens, and/or serve as delivery agents [3-5]. Although only thirty Ab-

based drugs have received United States' Food and Drug Administration (US FDA) approval as of 2007, therapeutic Abs have had a nearly 100% acceptance rate following the successful completion of clinical trials [3-5]. Moreover, the development of the therapeutic Ab drug pipeline has proven to be profitable: five of the top ten biotechnological drugs of 2007 were Abs, with projected annual sales of $3-5 billion US [3-5]. Currently, there are approximately three hundred therapeutic Abs, and their derivatives, in clinical trials [3-5]. Clearly, therapeutic Abs are a promising field of research and development, both medically and economically.

The current approaches to therapeutic Ab production include the isolation and screening of large ASC populations from humans or transgenic mice (specifically, genetically modified mice whose deoxyribonucleic acid (DNA) has been altered to carry the human genes encoding the said Abs), from which Abs targeting a specific Ag with the highest affinities are identified. The genes encoding the expressed Abs are then cloned and transferred into Ab-expression DNA vectors, which are then used to transform cultured cell lines into ASC lines that produce large quantities of the desired Ag-specific Abs [6,7].

To identify the ASCs that produce high-affinity Ag-specific Abs, hundreds-to-thousands of ASCs are typically screened. These ASCs are typically hybridoma cell lines [8,9] that are produced by fusing human or murine B cells to myeloma cells. These fused cells are cultured to form stable cell lines, and the culture supernatants are tested for the presence of Ag-specific Abs. As the B cells used to create the hybridoma cell lines often do not produce Ag-specific Abs, large populations of ASCs must be screened to identify high-affinity Ag-specific Abs with the desired biological characteristics. Whilst this approach produces a significant volume of Ab for up-front testing prior to selecting the ASCs to clone, it also suffers from significant drawbacks, including the labour-intensive production and screening of thousands of ASC lines (a process that typically requires 4-6 weeks to obtain 1-10 clonal cell lines of interest).

We are contributing to a multidisciplinary project focused upon developing an immunobiosensing array to directly monitor the Ab production by thousands of ASCs on a single slide, which would afford the real-time identification of the ASCs that produce the desired Ag-specific Abs with the strongest affinities. Genes encoding the expressed Abs can be cloned by using the ASCs' messenger ribonucleic acid (mRNA) to produce complementary DNA (cDNA) from which Ab-encoding cDNA sequences can be isolated and amplified, cloned into Ab-expression vectors, and subsequently used to transform cultured cells into ASC lines that produce the desired Ag-specific Abs.

Our contribution to this project involves trapping single ASCs near individual Ab sensors composed of a thin gold (Au) film milled, *via* a focused ion beam, with arrays of nanoholes onto which Ag has been immobilized. The nanohole arrays are optically excited to produce collective electronic oscillations, known as surface plasmons (SPs) [10-14], which yield surface-bound electromagnetic fields. This SP resonance (SPR) depends upon the dielectric contrast at the metal-dielectric interface, and is thus sensitive to changes to the refractive index near the Au surface as induced by molecular adsorption (*e.g.* as induced by the specific binding of Abs to the immobilized Ag). This sensitivity has been widely exploited within chemical, biochemical, and biomedical sensing technologies to monitor various surface binding events [15,16]. Our project follows the binding of secreted Abs to the immobilized Ag, which alters the optical transmission through the associated nanohole array *via* changes in its SPR. The Ag-specific affinities of the Abs secreted by each ASC can be deduced by monitoring the rates of Ab binding and release from the immobilized Ag (referred to as the on- and off-rates, respectively) *via* the optical transmission through each associated nanohole array. These on- and off-rates are to be monitored across the entire slide, which contains many nanohole array based Ag-specific Ab sensors.

Before we can perform these secreted Ab affinity measurements on such a large scale, we must first develop a system capable of trapping large ASC populations within arrays of single-cell traps. The manipulation of individual biological cells has been a major focus of microfluidics research [17]. Most relevant to our project, researchers have trapped large cellular populations within arrays of microstructures intended to trap single cells [18-20]. For example, Lee *et al.* report cup microstructures whose concave openings face an oncoming fluid flow, trapping cells suspended within the flowing fluid *via* perfusion [18]. Moreover, Love *et al.* and Muraguchi *et al.* both report arrays of microwells which trap fluid-suspended cells settling under the influence of gravity [19,20].

We have previously reported the integration of nanohole arrays with polymeric microfluidic channels [21]. Since then, we have been developing polymeric microfluidic systems with which to trap large ASC populations within arrays of single-cell traps, as inspired by the successes of Lee *et al.*, Love *et al.*, and Muraguchi *et al.* [18-20]. Each of our cell trap designs were fabricated using SU-8 photoresist [22] and poly(dimethyl siloxane) (PDMS) [23], and tested using polystyrene microspheres (PSS) [24] and the hybridoma cell line 17/9 [25,26], which secretes a peptide-binding Ab. This paper presents our initial work developing these various polymeric arrays of single-cell traps.

FLOW-THROUGH CELL TRAPS

Figure 1 presents our first flow-through cell trap design, inspired by the success of the u-shaped cup microstructures reported by Lee *et al.* [18]. The fluid flow is intended to carry a given suspended cell into the concave opening of one of these cup traps. The 10 μm wide channel bisecting each cup trap is intended to be too narrow to afford further cellular passage, trapping the aforementioned cell against the fluid flow *via* perfusion.

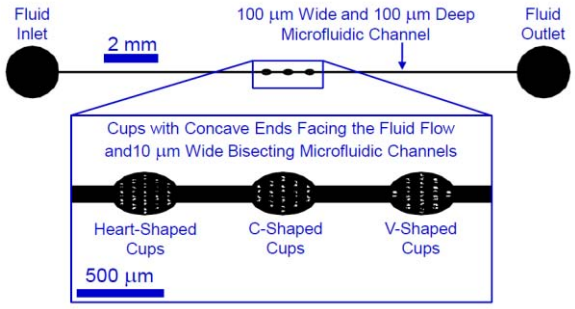

Figure 1: Fluid-suspended cells are carried into the concave openings of various cup trap microstructures. The 10 μm wide channel bisecting each cup trap is intended to be too narrow to afford further cellular passage, trapping the said cells *via* perfusion.

Figure 2 presents our second flow-through cell trap design, which builds upon the aforementioned perfusive single-cell trapping principal with the addition of 50-μm-by-50-μm chambers connected to a given cup trap's bisecting channel *via* additional channels that are also too narrow to permit further cellular passage. The Ab-sensing nanohole arrays are to be sheltered within these chambers, so as to be exposed to the Abs secreted by the nearby trapped ASC whilst being largely shielded from the Abs secreted by other ASCs. Given their intended function, these chambers shall hereto be referred to as nanohole array shelters.

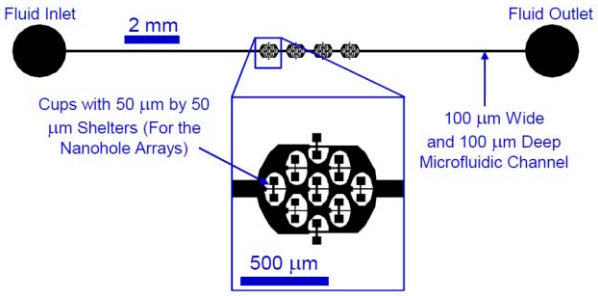

Figure 2: Cup-based flow-through cell traps featuring 50-μm-by-50-μm nanohole array shelters connected *via* additional channels that are also too narrow to permit further cellular passage.

Figures 3-5 present our other flow-through cell trap designs. Unlike the design depicted in Figure 2, the cup traps and nanohole array shelters depicted in Figures 3-5 are inset into the walls of curved microfluidic channels. Based upon the expectation that the cells shall be denser than the fluid medium in which they are suspended: centrifugal force $\boldsymbol{F_c}$ should push these cells out to the channels' perimeter, where the fluid flow should then carry these cells into the concave openings of the cup traps inset into the channels' walls.

Figure 3 presents a flow-through cell trap design in which cup traps and nanohole array shelters are inset into the walls of a serpentine microfluidic channel's bends. This design is inspired by the serpentine-shaped microfluidic channels commonly utilized as microfluidic mixers [27], capitalizing on the back and forth motion of the normally laminar microfluidic flow as induced by $\boldsymbol{F_c}$. As previously mentioned, $\boldsymbol{F_c}$ shall push cells towards the channel's walls. However, the wall to which $\boldsymbol{F_c}$ pushes cells towards changes following a bend. Consequently, it is probable that only the cells flowing near the walls of the initial bends would be trapped. Regardless, the relative commonness of the serpentine microfluidic channel lends itself as a logical comparison to the other designs in which cup traps are inset into a curved microfluidic channel's walls.

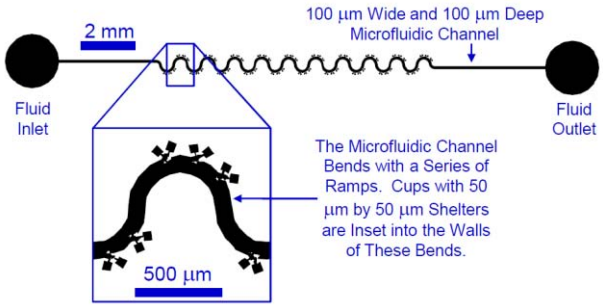

Figure 3: Flow-through cell cup traps and nanohole array shelters inset into the walls of a serpentine microfluidic channel.

Figure 4 presents a flow-through cell trap design in which cup traps and nanohole array shelters are inset into the walls of a ramped microfluidic channel's inter-bend straight runs. As with the serpentine channel, the wall to which $\boldsymbol{F_c}$ pushes cells towards changes following a bend and as such it is probable that only the cells flowing near the walls of the initial straight runs would be trapped. Regardless, the placement of the cup traps along the inter-bend straight runs makes this design a logical perturbation of the serpentine channel depicted in Figure 3.

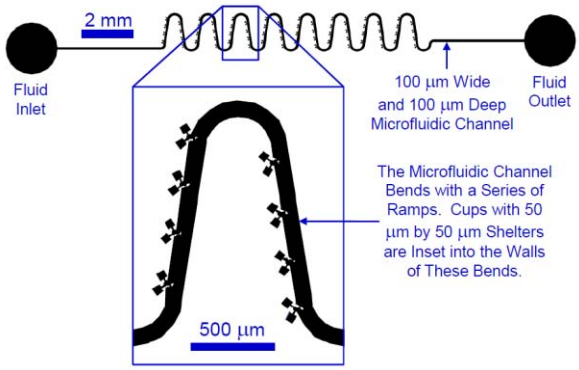

Figure 4: Flow-through cell cup traps and nanohole array shelters inset into the walls of a ramped microfluidic channel.

Figure 5 presents a flow-through cell trap design in which cup traps and nanohole array shelters are inset into the walls of a spiraled microfluidic channel. Unlike the serpentine and ramped microfluidic channels depicted in Figures 3-4, $\boldsymbol{F_c}$ shall continuously push the suspended cells towards the same wall. As such, this spiraled design is expected to have an improved trapping efficiency and moreover cells are increasingly likely to become trapped within the innermost turns. For these reasons, the spiraled design is a logical comparison to the serpentine and ramped designs depicted in Figures 3-4.

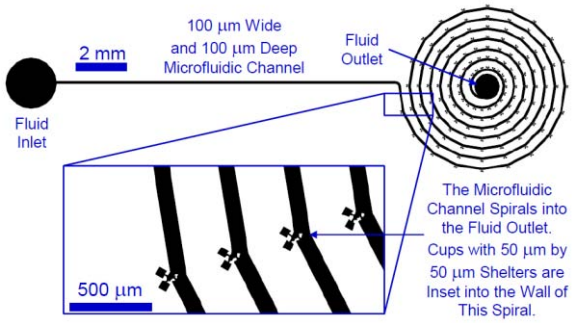

Figure 5: Flow-through cell cup traps and nanohole array shelters inset into the walls of a spiraling microfluidic channel.

Within the following sub-section, each of the flow-through cell trap designs depicted in Figures 1-5 are modeled and evaluated using COMSOL® Multiphysics [28]. These simulations indicated that these five flow-through cell trap designs were worthy of further consideration, whereas other flow-through cell trap designs (which are not presented within this paper) were shown to be unworthy of further consideration and were thus abandoned. The remaining sub-sections discuss the fabrication and preliminary flow-based testing of each of the flow-through cell trap designs depicted in Figures 1-5.

SIMULATION OF FLOW-THROUGH CELL TRAPS

The fluid velocity $\boldsymbol{v}_f$ profiles within each of the flow-through cell trap designs depicted in Figures 1-5 were simulated within COMSOL® Multiphysics 2D Incompressible Navier-Stokes Module [28] using: a 100 μm deep shallow channel approximation, pressure P boundary conditions (BCs) at the fluid inlet and outlet, and no-slip BCs along the microfluidic channels' perimeter. Cellular trajectories within these simulated $\boldsymbol{v}_f$ profiles were then estimated *via* $\boldsymbol{v}_f$ streamlines and particle tracing simulations. Mesh independence was assured within each of these simulations.

Due to computational memory constraints, the entirety of the designs depicted in Figures 1-5 were not modeled. For example, neither the nanohole array shelters nor their connecting channels were included within any of these models. However, as the fluid flows through these regions are expected to be minimal, the errors within the simulated $\boldsymbol{v}_f$ profiles due to the absence of the nanohole array shelters and their connecting channels are expected to be negligible.

Figures 6-8 respectively present the simulated $\boldsymbol{v}_f$ profiles within the heart-, C-, and V-shaped cup traps depicted in Figure 1. Each of these simulations only modeled part of the entire array of cup traps depicted in Figure 1, using a simplified geometry of 9-12 cups within a single chamber centered upon a 9 mm long and 100 μm wide channel. These simulations were initialized using 20 Pa inlet-outlet pressure differential ΔP BCs. Well known analytical flow rate calculations [29], based upon fluidic resistance, estimate that these ΔP = 20 Pa BCs yield laminar, parabolic Poiseuille $\boldsymbol{v}_f$ profiles, with a mean $|\boldsymbol{v}_f| \approx 0.9$ mm/s within the main 100 μm wide channels. These analytical predictions are verified by Figures 6-8, in which the mean $|\boldsymbol{v}_f|$ within the main 100 μm wide channels are approximately 1, 0.9, and 1 mm/s, respectively.

Figures 6-8 each demonstrate that the $\boldsymbol{v}_f$ streamlines flow through several of the cup traps, suggesting that the fluid-suspended cells would likely be trapped at the concave openings of these cup traps (assuming that their bisecting channels will not afford further cellular passage). Furthermore, $|\boldsymbol{v}_f|$ is relatively low near the concave openings of these cup traps, suggesting that the fluid drag forces experienced by the trapped cells would be minimal.

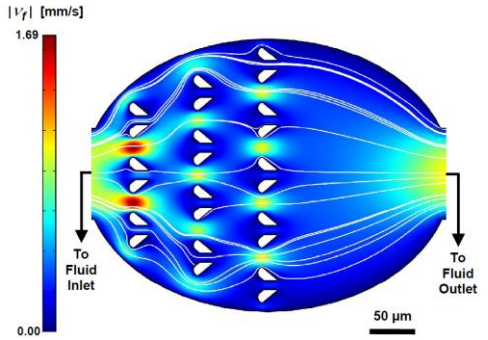

Figure 6: The $\boldsymbol{v}_f$ field (colour) and streamlines (white) within the heart-shaped cup traps depicted in Figure 1 (at t = 30 s), as simulated using COMSOL® Multiphysics with ΔP = 20 Pa and 20 streamlines.

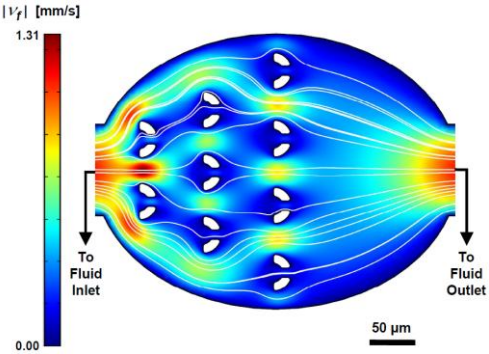

Figure 7: The $\boldsymbol{v}_f$ field (colour) and streamlines (white) within the C-shaped cup traps depicted in Figure 1 (at t = 30 s), as simulated using COMSOL® Multiphysics with ΔP = 20 Pa and 20 streamlines.

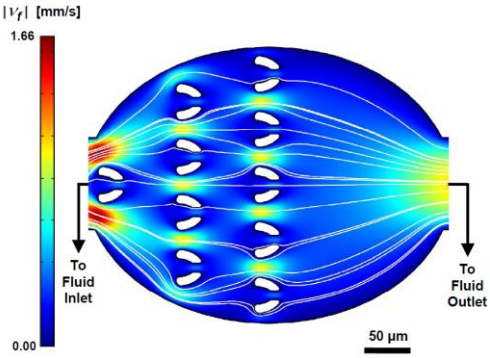

Figure 8: The $\boldsymbol{v}_f$ field (colour) and streamlines (white) within the V-shaped cup traps depicted in Figure 1 (at t = 30 s), as simulated using COMSOL® Multiphysics with ΔP = 20 Pa and 20 streamlines.

Figure 9 presents the simulated $\boldsymbol{v}_f$ profile within the cup traps depicted in Figure 2. This simulation only modeled part of the entire array of cup traps depicted in Figure 2, using a simplified geometry of five shelter-less cups within a single chamber centered upon a 9 mm long and 100 μm wide channel. This simulation was also initialized using a ΔP = 20 Pa BC. As such, the fluidic resistance based analytical flow rate calculations [29] again imply a laminar, parabolic Poiseuille $\boldsymbol{v}_f$ profile, with a mean $|\boldsymbol{v}_f|$ ≈ 0.9 mm/s within the main 100 μm wide channel. This analytical prediction is verified by Figure 9, in which the mean $|\boldsymbol{v}_f|$ within the main 100 μm wide channel is approximately 0.9 mm/s.

Figure 9 demonstrates that the $\boldsymbol{v}_f$ streamlines mostly flow around the cup traps, with only five of the thirty plotted $\boldsymbol{v}_f$ streamlines passing directly through the cup traps' bisecting channels. This suggests that the fluid-suspended cells would likely not be trapped at the concave openings of these cup traps. Notably, the poorer fluidic performance of these cup traps may be overshadowed by the Ab shielding advantages provided by the nanohole array shelters. As such, these cup traps were not immediately abandoned on the basis of their relatively poor fluidic simulation performance alone.

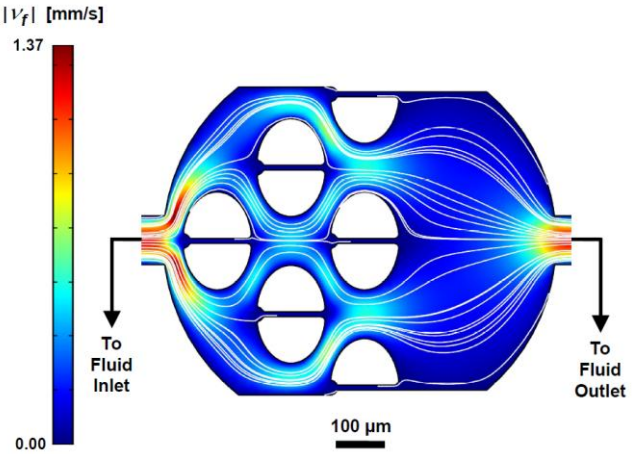

Figure 9: The $\boldsymbol{v}_f$ field (colour) and streamlines (white) within the cup traps depicted in Figure 2 (at t = 30 s), as simulated using COMSOL® Multiphysics with ΔP = 20 Pa and 30 streamlines.

Figure 10 presents the simulated $\boldsymbol{v}_f$ profile within the serpentine channel depicted in Figure 3. This simulation only modeled part of the entire channel depicted in Figure 3, using a simplified geometry of four shelter-less serpentine bends within a 10 mm long and 100 μm wide channel. This simulation was initialized using a ΔP = 15 Pa BC. As such, the fluidic resistance based analytical flow rate calculations [29] imply a laminar, parabolic Poiseuille $\boldsymbol{v}_f$ profile, with a mean $|\boldsymbol{v}_f|$ ≈ 0.6 mm/s within the main 100 μm wide channel. This analytical prediction is verified by Figure 10, in which the mean $|\boldsymbol{v}_f|$ within the main 100 μm wide channel is approximately 0.7 mm/s.

Figure 10 demonstrates that the $\boldsymbol{v}_f$ streamlines flow through each of the twelve cup traps, suggesting that fluid-suspended cells would likely be trapped at the concave openings of these cup traps (under the assumptions that the suspended cells shall be denser than the fluid medium and that the cup traps' bisecting channels will not afford further cellular passage). Moreover, $|\boldsymbol{v}_f|$ is relatively low near the concave openings of these cup traps, suggesting that the fluid drag forces experienced by the trapped cells would be minimal.

However, only the 1-2 streamlines nearest a given wall pass through the cup traps along that said wall. The streamlines further away from the walls are not pushed outwards as they traverse the serpentine channel. This suggests that only the cells sufficiently close to a wall would be trapped.

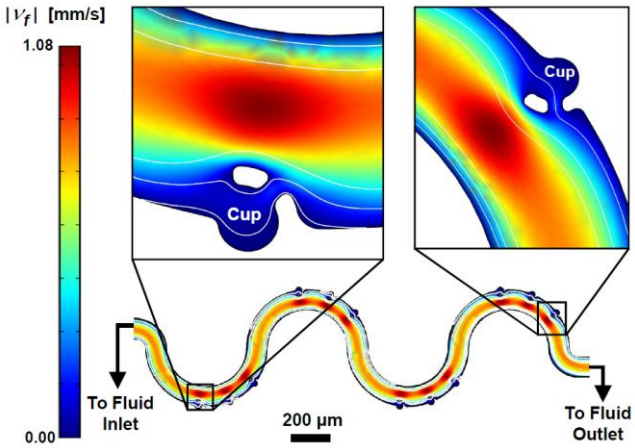

Figure 10: The $\boldsymbol{v}_f$ field (colour) and streamlines (white) within the cup traps depicted in Figure 3 (at t = 30 s), as simulated using COMSOL® Multiphysics with ΔP = 15 Pa and 12 streamlines.

Figure 11 presents the simulated $\boldsymbol{v}_f$ profile within the ramped channel depicted in Figure 4. This simulation only modeled part of the entire channel depicted in Figure 4, using a simplified geometry of four shelter-less ramps within an approximately 11 mm long and 100 μm wide channel. This simulation was initialized using a ΔP = 20 Pa BC. As such, the fluidic resistance based analytical flow rate calculations [29] imply a laminar, parabolic Poiseuille $\boldsymbol{v}_f$ profile, with a mean $|\boldsymbol{v}_f|$ ≈ 0.7 mm/s within the main 100 μm wide channel. This analytical prediction is verified by Figure 11, in which the mean $|\boldsymbol{v}_f|$ within the main 100 μm wide channel is approximately 0.8 mm/s.

Figure 11 demonstrates that the $\boldsymbol{v}_f$ streamlines pass through only three of the sixteen simulated cup traps, suggesting that the fluid-suspended cells would likely not be trapped at the concave openings of these cup traps. However, it was observed that the $\boldsymbol{v}_f$ streamlines pass through more of these simulated cup traps as ΔP, and thus $|\boldsymbol{v}_f|$, increases. Moreover, $|\boldsymbol{v}_f|$ is relatively low near the concave openings of these cup traps, suggesting that the fluid drag forces experienced by the trapped cells would be minimal. As such, these cup traps were not immediately abandoned on the basis of their relatively poor ΔP = 20 Pa fluidic simulation performance alone.

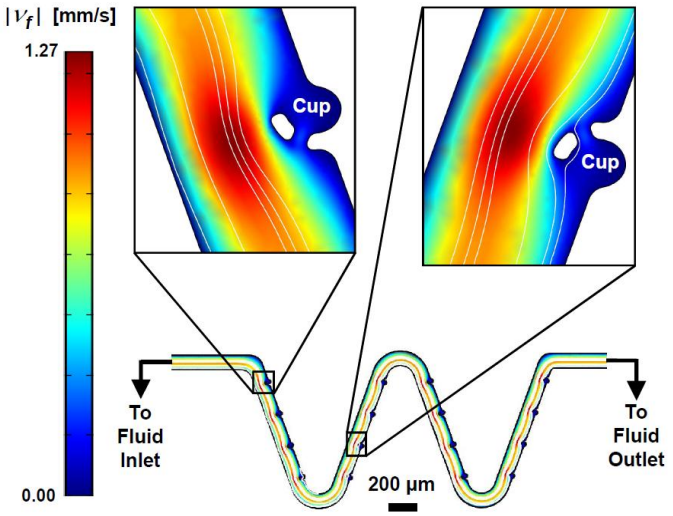

Figure 11: The v_f field (colour) and streamlines (white) within the cup traps depicted in Figure 4 (at t = 30 s), as simulated using COMSOL® Multiphysics with ΔP = 20 Pa and 8 streamlines.

Figure 12 presents the simulated v_f profile within the spiraled channel depicted in Figure 5. This simulation only modeled part of the entire channel depicted in Figure 5, using a simplified geometry of two and a half shelter-less turns within an approximately 10 mm long and 100 µm wide channel. This simulation was initialized using a ΔP = 20 Pa BC. As such, the fluidic resistance based analytical flow rate calculations [29] imply a laminar, parabolic Poiseuille v_f profile, with a mean $|v_f|$ ≈ 0.8 mm/s within the main 100 µm wide channel. This analytical prediction is verified by Figure 12, in which the mean $|v_f|$ within the main 100 µm wide channel is approximately 0.9 mm/s.

Figure 12 demonstrates that the v_f streamlines near the channel's outer perimeter flow through the cup traps following the spiral's first half-turn, suggesting that the fluid-suspended cells would likely be trapped at the concave openings of these cup traps (under the assumptions that the suspended cells shall be denser than the fluid medium and that the cup traps' bisecting channels will not afford further cellular passage). Moreover, $|v_f|$ is relatively low near the concave openings of these cup traps, suggesting that the fluid drag forces experienced by the trapped cells would be minimal. It is assumed that this trend of cells being trapped after the spiral's first half-turn would be extended within the complete design depicted in Figure 5, which contains seven turns rather than two and a half turns.

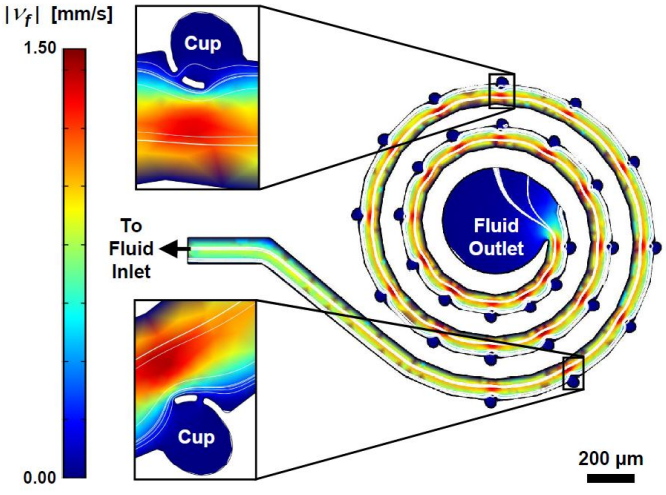

Figure 12: The v_f field (colour) and streamlines (white) within the cup traps depicted in Figure 5 (at t = 30 s), as simulated using COMSOL® Multiphysics with ΔP = 20 Pa and 20 streamlines.

The effects of varying the ΔP BCs, and thus varying the resulting v_f fields, were also examined within these simulations. As a specific example, Figure 13 presents the spiraled channel simulation re-run with a ΔP BC of 200 Pa, rather than the 20 Pa used previously. The fluidic resistance based analytical flow rate calculations [29] now imply a laminar, parabolic Poiseuille v_f profile, with a mean $|v_f|$ ≈ 8 mm/s within the main 100 µm wide channel. This analytical prediction is verified by Figure 13, in which the mean $|v_f|$ within the main 100 µm wide channel is approximately 9 mm/s.

The general behavior of the v_f streamlines presented in Figure 13 is similar to those presented in Figure 12. However, at the higher ΔP of Figure 13: the v_f streamlines were observed to be more concentrated near the outer perimeter of the spiraled channel, and thus more v_f streamlines passed through the cup traps inset into the channel wall, implying an increased cell trapping efficiency. This same behavior of increased v_f streamline density at the channels' outer perimeters with increased ΔP, and thus increased trapping efficiency as implied by the increased number of v_f streamlines passing through the cup traps, was also observed within the simulated ramp and serpentine channels.

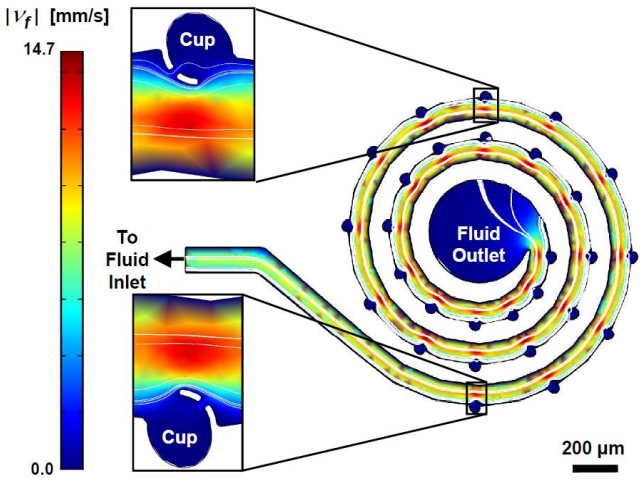

Figure 13: The v_f field (colour) and streamlines (white) within the cup traps depicted in Figure 5 (at t = 30 s), as simulated using COMSOL® Multiphysics with ΔP = 200 Pa and 20 streamlines.

The simulated v_f streamlines within Figures 6-13 suggest that the flow-through cell traps depicted in Figures 1, 3, and 5 should trap cells more efficiently than the flow-through cell traps depicted in Figures 2 and 4, for a given ΔP. Furthermore, $|v_f|$ is relatively low near the concave openings of all of the cup traps depicted in Figures 6-13, suggesting that the fluid drag forces experienced by the trapped cells would be minimal in the trap areas. Notably, the assumption that the v_f streamlines accurately model cellular trajectories was confirmed using particle tracing simulations within the simulated v_f fields.

FABRICATION OF FLOW-THROUGH CELL TRAPS

The flow-through cell traps were fabricated using: 1"-by-1.5", 1"-by-3", and 3"-by-3" RCA cleaned soda-lime glass slides with and without 5 nm thick titanium (Ti) or chrome (Cr) adhesion layers, RCA cleaned 4" diameter Pyrex wafers, and RCA cleaned 4" diameter silicon (Si) wafers. 30-122 µm thick films of MicroChem's SU-8 2035 photoresist [22] were first spun onto these substrates. These films were then immediately soft-baked on a 65°C hot-plate. Following this soft-bake, each SU-8 film's edge-bead was removed using acetone. Each SU-8 film was then photolithographically patterned using a Mylar contact mask containing each of the flow-through cell trap designs depicted in Figures 1-5. These SU-8 films were then post-exposure baked on a 95°C hot-plate. MicroChem's SU-8 photoresist developer was then used to develop these SU-8 films. The spin speeds, soft-baking times, optical exposure times, and post-exposure baking times used throughout this fabrication process were determined by the desired SU-8 film thicknesses as based upon parameters listed in MicroChem's SU-8 2025-2075 datasheet [22], which were subsequently optimized for our laboratory's equipment. The end of SU-8 development was determined manually *via* visual inspection.

Some of the SU-8 films were instead patterned with the negative of the aforementioned Mylar contact mask, to create molds that were subsequently used to fabricate each of the flow-through cell traps depicted in Figures 1-5 using Dow Corning's Sylgard® 184 poly(dimethyl siloxane) (PDMS) [23] (*via* a soft-lithographic process similar to the those described in [30,31]). The surface of these PDMS films were not activated with oxygen (O_2) plasma prior to the preliminary tests discussed in the following sub-section.

One notable problem encountered during the fabrication of the flow-through cell traps using SU-8 was the poor adhesion of 10-15 µm wide structures to the substrate (as seen in Figure 14). This lack of adhesion was partially reduced when the SU-8 film was no thicker than 50 µm, when the substrate had a 5 nm thick Ti or Cr adhesion layer, when the substrate's surface area was reduced, and/or when a Si or Pyrex substrate was used instead of soda-lime glass. The fabrication of the flow-through cell traps using PDMS afforded an improved small feature definition, and as such did not suffer from the aforementioned lack of small structure adhesion to the substrate that was observed when fabricating the flow-through cell traps using SU-8. However, the fabricated PDMS features were occasionally smaller than expected, likely due to PDMS shrinkage and/or poor SU-8 mold definition. Consequently, cells were occasionally able to pass through the bisecting channels and nanohole array shelter channels that were intended to be too narrow to afford further cellular passage (as will be seen in Figure 15).

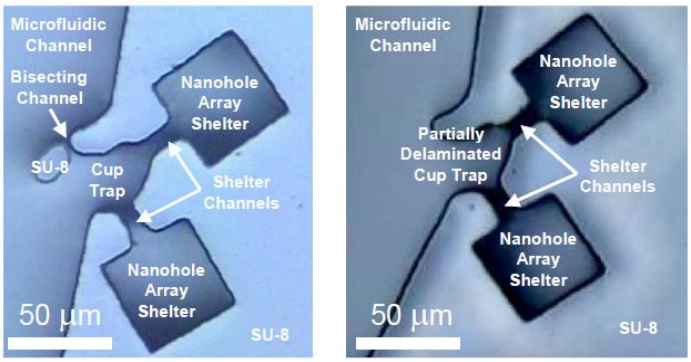

Figure 14: Flow-through cell trap cups and nanohole array shelters fabricated using SU-8. The cup trap on the right suffered from partial delamination, due to the poor adhesion of small features to the substrate observed when using SU-8.

TESTING OF FLOW-THROUGH CELL TRAPS

The flow-through cell traps were experimentally tested using 20 µm diameter polystyrene microspheres (PSS) [24] suspended in deionized water (DI H_2O) and 10-20 µm diameter 17/9 hybridoma cells [15,26] suspended in Dulbecco's modified Eagle's medium (DMEM). The 17/9 hybridoma cells' behaviour during these preliminary tests are expected to mimic the behaviour that would be observed with the B cells. Concentrations on the order of 10^5 cells-or-PSS/mL and flow rates on the order of tens of µL/min were utilized throughout these tests.

Most cells were observed to flow around the SU-8 cup traps, with few becoming trapped within the cup's concave

openings. The observed inefficiency of our cell trapping may be due to the reduction in fluid flow through the cup traps' bisecting channels as a result of poor SU-8 cup trap adhesion to the substrate.

The flow-through cell traps within the serpentine and spiraled channels yielded the best trapping efficiencies, as predicted by our aforementioned simulations using COMSOL® Multiphysics. Moreover, the flow-through cell traps were found to yield improved trapping efficiencies when fabricated using PDMS instead of SU-8.

However, our flow-through cell trap designs and our experimental methods must be further refined to ultimately yield the desired arrays of single-cell traps capable of reversibly trapping large ASC populations on a single slide. Figure 15 presents a PSS trapped within a cup trap inset into the wall of a spiraled channel fabricated using PDMS. Moreover, Figure 15 also presents cells densely populated along the wall of a serpentine channel fabricated using PDMS, alongside cells that were able to pass through nanohole array shelter channels. The removal of such extraneous cells has proven to be difficult using our current flow-through cell trap designs. However, we are tentatively planning to try various surface treatments and/or pressure bursting techniques which may facilitate the removal of these extraneous cells.

Moreover, we are also tentatively planning to try various hydrodynamic flow steering and/or cell sorting methods for the removal of the trapped ASCs, a step that will ultimately be necessary in order to prepare and amplify mRNA from the ASCs which produce Ag-specific Abs with the highest affinities.

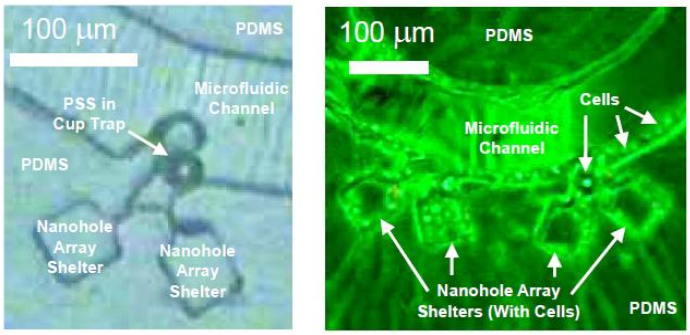

Figure 15: (LEFT) A PSS trapped in a flow-through cup trap inset into the wall of a spiraled channel fabricated using PDMS. (RIGHT) 17/9 hybridoma cells densely populated around the wall of a serpentine channel fabricated using PDMS, alongside cells that were able to pass through nanohole array shelter channels.

Cellular viability within the flow-through cell traps was evaluated following a 4 hour incubation period (during which the flow-through cell traps were placed within a 37°C incubator with a 5% carbon dioxide (CO_2) environment). The 17/9 hybridoma cells were found to be poisoned by the Cr adhesion layers; but appeared to remain healthy within all of our other fabricated flow-through cell traps. As such, to maintain cellular viability when using a substrate with an adhesion layer: Ti must be used instead of Cr. Moreover, we have previously demonstrated that SU-8 adheres more strongly to Ti than Cr [32].

MICROWELL ARRAY CELL TRAPS

Whilst flow-through cell traps are desirable from the standpoint of established hydrodynamic flow-based single-cell manipulation techniques, we are also investigating alternative methods with which to trap large ASC populations within arrays of single-cell traps. Inspired by the successes of Love *et al.* and Muraguchi *et al.* [19,20], we have developed cell traps composed of microwell arrays inset into the surface of a PDMS film. Our microwell array designs feature 30, 50, 100, and 200 µm circular topographic diameters, highly vertical sidewalls, and a 3.77 mm periodicity in both topographical directions. The following sub-sections discuss the fabrication and preliminary flow-based testing of the microwell array cell traps.

FABRICATION OF MICROWELL ARRAY CELL TRAPS

Our microwell array cell traps were fabricated using SU-8 and PDMS [22,23], *via* procedures similar to those used to fabricate our flow-through cell traps. Our fabricated arrays consisted of 60-80 µm deep microwells inset into the surface of 400-700 µm thick PDMS films. The surface of these PDMS films were not activated with O_2 plasma prior to the preliminary tests discussed in the following sub-section.

TESTING OF MICROWELL ARRAY CELL TRAPS

As with our flow-through cell traps, our microwell array cell traps were experimentally tested using 10-20 µm diameter 17/9 hybridoma cells [25,26] suspended in culture medium (*i.e.* DMEM). These preliminary cell trapping experiments were adapted from a protocol outlined by Love *et al.* [20].

Suspensions of $4x10^5$ 17/9 hybridoma cells/mL of DMEM were deposited onto the surface of our PDMS films (more specifically, approximately 100 µL of the cellular suspension were deposited onto the quadrants of the PDMS films containing the 200 µm diameter microwells). We observed that the 200 µm diameter microwells would typically fill with 5-20 cells during a 10 minute settling time. Figure 16 presents micropictographs of a representative 200 µm diameter microwell immediately prior to cellular deposition and approximately 5 and 10 minutes after cellular deposition. Using a peristaltic pump, we then successfully removed the cells outside of the microwells whilst minimizing the displacement of the cells trapped within the microwells (as shown in Figure 16). Figure 16 also demonstrates the viability of the trapped cells within the microwells following approximately 4, 6, and 24 hours of incubation (at 37°C within a 5% CO_2 environment). In contrast to the success of the microwell arrays fabricated using PDMS, we had significant difficulty trapping cells within the microwells fabricated using SU-8, possibly due to SU-8's surface charge or hydrophobicity.

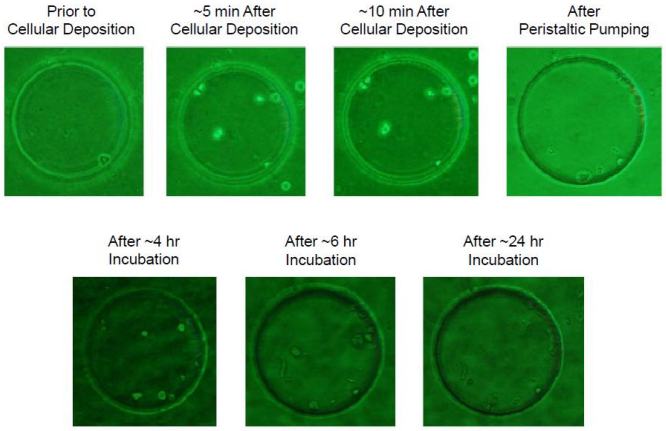

Figure 16: 17/9 hybridoma cells falling into a 200 μm diameter and 60-80 μm deep microwell fabricated using PDMS during a 10 min settling period. A peristaltic pump was used to remove cells outside of the microwells whilst minimizing the displacement of the cells trapped within the microwells. These trapped cells appeared to be viable following a 24 hour incubation at 37°C in a 5% CO_2 environment.

Although we are encouraged by the preliminary results of our microwell array tests, further refinements to our design and experimental procedures are necessary to ultimately yield arrays of single-cell traps capable of reversibly trapping large ASC populations on a single slide. This refinement could conceivably be as simple as empirically tailoring the deposited cellular concentration until an average of 1-3 cells are trapped within a given microwell. Moreover, we are also tentatively planning to remove trapped ASCs using micropipetting techniques.

CONCLUSIONS

We have designed, simulated, fabricated, and performed preliminary experimental tests on a variety of first-generation arrays of single-cell traps to ultimately be used for trapping large ASC populations. The basic perfusive cell trapping principle of our flow-through cell traps, fabricated using SU-8 and PDMS [23,24], has been verified *via* COMSOL® Multiphysics [28] simulations and experimental testing using fluid-suspended PSS [24] and 17/9 hybridoma cells [25,26]. Experimental testing using fluid-suspended 17/9 hybridoma cells has also verified the functionality of our microwell array traps fabricated using PDMS.

Although we are encouraged by our preliminary results, our flow-through cell trap designs and/or experimental methods must be further refined to ultimately yield arrays of single-cell traps capable of reversibly trapping large ASC populations on a single slide. However, the deposited cellular concentration could conceivably be empirically tailored to achieve this performance using our microwell array traps, as the results of their preliminary tests are more promising by comparison.

It is necessary to remove extraneous cells in the vicinity of a trapped single cell, so as to isolate a given nanohole array from the Abs secreted by ASCs other than the nearby trapped ASC of interest. The removal of such extraneous cells will require further refinements to our flow-through cell trap designs and/or experimental methods, including further surface chemistry and/or hydrodynamic flow manipulation considerations. However, using a peristaltic pump, we have successfully removed extraneous cells outside of the microwells whilst minimizing the displacement of the cells trapped within the microwells.

It shall also be necessary to remove the trapped ASCs, in order to prepare and amplify mRNA from the ASCs which produce Ag-specific Abs with the highest affinities. In the case of our flow-through cell traps, we are tentatively planning to try various hydrodynamic flow steering and/or cell sorting methods to remove the trapped ASCs. In the case of our microwell array traps, we are tentatively planning on using a micropipetting procedure to remove the trapped ASCs.

We consider our progress thus far to be a good start towards our ultimate goal of designing a microfluidic system capable of trapping thousands of ASCs within arrays of single-cell traps on a single slide, each of which is in the vicinity of a designated nanohole array for secreted Ag-specific Ab detection.

ACKNOWLEDGMENTS

We thank our colleagues working alongside us to develop this immunobiosensing system: Karen L. Kavanagh, Donna Hohertz, Alexandre G. Brolo, Rajinder Nirwan, Christy Hui, Reuven Gordon, and Jody Berry. We also thank Jasbir N. Patel, Ajit Khosla, and Bill Woods for their assistance during the fabrication of the devices presented in this paper. We also acknowledge the finance and resources provided by the Canadian Microelectronics Corporation (CMC), the Natural Sciences and Engineering Research Council of Canada (NSERC), the Canada Foundation for Innovation (CFI), and the British Columbia Knowledge Development Fund (BCKDF).

REFERENCES

[1] Ahmed, R., and Gray, D., 1996, "Immunological memory and protective immunity: understanding their relation", *Science*, **272**, pp. 54-60.

[2] Sifka, M.K., and Ahmed, R., 1998, "Long-lived plasma cells: a mechanism for maintaining persistent antibody production", *Curr. Opin. Immunol.*, **10**, pp. 252-258.

[3] Piggee, C., 2008, "Therapeutic antibodies coming through the pipeline", *Anal. Chem.*, **80**, pp. 2305-2310.

[4] Lawrence, S., 2007, "Pipelines turn to biotech.", *Nat. Biotechnol.*, **25**, pp. 1342.

[5] Baker, M., 2005, "Upping the ante on antibodies', *Nat. Biotechnol.*, **23**, pp. 1065-1072.

[6] Babcook, J.S., Leslie, K.B., Olsen, O.A., Salmon, R.A., and Schrader, J.W., 1996, "A novel strategy for generating monoclonal antibodies from single, isolated lymphocytes producing antibodies of defined specificities", *Proc. Natl. Acad. Sci. USA*, **93**, pp. 7843-7848.

[7] Dessain, S.K., Adekar, S.P., and Berry, J.D., 2008, "Exploring the native human antibody repertoire to create antiviral therapeutics", *Human Antibody Therapeutics for Viral Disease: Current Topics in Microbiology and Immunology*, Dessain, S.K. (ed.), Springer-Verlag, Berlin, Germany, **317**, pp. 155-183.

[8] Dessain, S.K., Adekar, S.P., Stevens, J.B., Carpenter, K.A., Skorski, L.M., Barnoski, B.L., Goldsby, R.A., and Weinberg, R.A., 2004, "High efficiency creation of human monoclonal antibody-producing hybridomas", *J. Immunol. Meth.*, **291**, pp. 109-122.

[9] Lanzaecchia, A., Corti, D., and Sallusto, F., 2007, "Human monoclonal antibodies by immortalization of memory B cells", *Curr. Opin. Biotechnol.*, **18**, pp. 523-528.

[10] Raether, H., 1988, *Surface Plasmons on Smooth and Rough Surfaces and on Gratings: Springer Tracts in Modern Physics*, Springer-Verlag, Berlin, Germany, **111**, pp. 1-136.

[11] Lal, S., Link, S, Halas, N.J., 2007, "Nano-optics from sensing to waveguiding", *Nature Photonics*, **1**, pp. 641-648.

[12] Barnes, W.L., Dereux, A., Ebbesen, T.W., 2003, "Surface plasmon subwavelength optics", *Nature*, **424**, pp. 824-830.

[13] Maier, S.A., Atwater, H.A., 2005, "Plasmonics: localization and guiding of electromagnetic energy in metal/dielectric structures", *J. Appl. Phys.*, **98**(011101), pp. 1-10.

[14] Sharpe, J.C., Mitchell, J.S., Lin, L., Sedoglavich, N., and Blaikie, R.J., 2008, "Gold nanohole array substrates as immunobiosensors", *Anal. Chem.*, **80**, pp.2244-2249.

[15] Homola, J., 2008, "Surface plasmon resonance sensors for detection of chemical and biological species", *Chem. Rev.*, **108**, pp. 462-493.

[16] Stewart, M.E., Anderton, C.R., Thompson, L.B., Maria, J., Gray, S.K., Rogers, J.A., Nuzzo, R.G., 2008, "Nanostructured plasmonic sensors", *Chem. Rev.*, **108**, pp. 494-521.

[17] Andersson, H., and van den Berg, A., 2003, "Microfluidic devices for cellomics: a review", **92**, pp. 315-325.

[18] Di Carlo, D., Wu, L.Y., and Lee, L.P., 2006, "Dynamic single cell culture array", **6**, pp. 1445-1449.

[19] Tokimitsu, Y., Kishi, H., Kondo, S., Honda, R., Tajiri, K., Motoki, K., Ozawa, T., Kadowaki, S., Obata, T., Fujiki, S., Tateno, C., Takaishi, H., Chayama, K., Yoshizato, K., Tamiya, E., Sugiyama, T., and Muraguchi, A., 2007, "Single lymphocyte analysis with a microwell array chip", *Cytometry Part A*, **71A**, pp. 1003-1010.

[20] Ogunniyi, A.O., Story, C.M., Papa, E., Guillen, E., and Love, J.C., 2009, "Screening individual hybridomas by microengraving to discover monoclonal antibodies", *Nature Protocols*, **4**, pp. 767-782.

[21] Westwood, S.M., Gray, B.L., Grist, S., Huffman, K., Jaffer, S., and Kavanagh, K., 2008, "SU-8 polymer enclosed microchannels with interconnect and nanohole arrays as an optical detection device for biospecies", *Proc. IEEE EMBC*, IEEE, Vancouver, British Columbia, Canada, pp. 5652-5655.

[22] MicroChem Corp., 2010, "SU-8 2000 permanent epoxy negative photoresist - processing guidelines for: SU-8 2025, SU-8 2035, SU-8 2050 and SU-8 2075", Product Processing Guidelines, Newton, Massachusetts, USA, *http://www.microchem.com/products/pdf/SU-82000DataSheet2025thru2075Ver4.pdf*.

[23] Dow Corning Corp., 2010, "Sylgard® 184 silicone elastomer kit", Product Documentation, Midland, Michigan, USA, *http://www.dowcorning.com/ /applications/search/default.aspx?R=131EN*.

[24] Polysciences, Inc., 2009, "Polybead® Microspheres", Technical Data Sheet 788, Warrington, Pennsylvania, USA, *http://www.polysciences.com/SiteData/docs/TDS% 20788/fa3c300bf743114f6efc0b6b377e6ec4/TDS% 20788.pdf*.

[25] Niman, H.L, Houghten, R.A., Walker, L.E., Reisfeld, R.A., Wilson, I.A., Hogle, J.M., and Lerner, R.A., 1983, "Generation of protein-reactive antibodies by short peptides in an event of high frequency: implications for the structural basis of immune recognition", *Proc. Natl. Acad. Sci. USA*, **80**(16), pp. 4949-4953.

[26] Rini, J.M., Schulze-Gahmen, U., and Wilson, I.A., 1992, "Structural evidence for induced fit as a mechanism for antibody-antigen recognition", *Science*, **255**, pp. 959-965.

[27] Song, H., Tice, J.D., and Ismagilov, R.F., 2003, "A microfluidic system for controlling reaction networks in time", *Angew. Chem. Int. Ed.*, **42**, pp. 767-772.

[28] COMSOL®, Inc., 2010, "COMSOL® Multiphysics modeling and simulation", Official Website, Burlington, Massachusetts, USA, *http://www.comsol.com*.

[29] White, F.M., 2010, *Fluid Mechanics (7th Ed.)*, McGraw-Hill, Whitby, Ontario, Canada, pp. 1-896.

[30] Gates, B.D., Xu, Q., Stewart, M., Ryan, D., Willson, C.G., and Whitesides, G.M., 2005, "New approaches to nanofabrication: molding, printing, and other techniques", *Chem. Rev.*, **105**, pp. 1171-1196.

[31] Xia, Y., Rogers, J.A., Paul, K.E., and Whitesides, G.M., 1999, "Unconventional methods for fabricating and patterning nanostructures", *Chem. Rev.*, **99**, pp.1823-1848.

[32] Grist, S., Patel, J.N., Haq, M., Gray, B.L., and Kaminska, B., 2010, "Effect of surface treatments/coatings and soft bake profile on surface uniformity and adhesion of SU-8 on a glass substrate", 75930F, *Proc. SPIE Photonics West*, SPIE, San Francisco, California, USA, **7593**, pp. 1-10.